

Optical Spectroscopy and Microscopy Studies on the Spatial Distribution and Reaction Dynamics in Zeolites

Shuichi Hashimoto*

Department of Ecosystem Engineering, The University of Tokushima, Tokushima 770-8506, Japan

ABSTRACT: This Perspective describes current research into the photochemistry of zeolites, pointing out issues yet to be resolved and suggesting future directions of investigation. The fascinating host materials are known to act as a support for guest ions, molecules, or clusters both within their large interior cage/channel networks and on their exterior surfaces, together providing rich chemistry. Two techniques have proven particularly successful for their study, diffuse reflectance transient absorption spectroscopy and optical microscopy. The various properties revealed by these techniques include intracrystalline and intercrystalline migration, migration-assisted photochemical reactions, and heterogeneous distribution of guest molecules among and within crystals.



Zeolites have been a target of scientific research for over 250 years, since their discovery in nature by an 18th-century mineralogist. Synthetic zeolites have played a leading role as catalysts in the past century and into this century.¹ In the past two decades, chemists have increasingly recognized that zeolites can act as superb molecular containers for supramolecular interactions, similar to micelles, microemulsions, and vesicles. This Perspective describes current research into the photochemistry of zeolites, pointing out issues yet to be resolved and suggesting areas for future investigation.

Supramolecular chemistry concerns the structure and dynamics of small ions, molecules, or clusters termed guests that are noncovalently bound to large molecules, molecular assemblies, or crystals termed hosts.² Zeolites are ideal hosts as their complex but strictly regular structures, reminiscent of a jungle gym (see TOC graphic), can accommodate guests into their void cages/cavities and channels. Photochemical studies reveal that the excited-state properties of guests are modified from their properties in solution due to constraints imposed by binding to the host. Product distributions of guests in the host thus differ from those in solution, enabling active control of host–species reaction pathways and kinetics.^{3–5}

Zeolites are ideal hosts as their complex but strictly regular structures can accommodate guests into their void cages/cavities and channels.

Zeolites have recently been used as a platform for nanotechnology.⁶ Two examples of this use include their possible role as a template for 3D superstructures consisting of CdS quantum dots⁷ and their role as an ETS-10 framework that can accommodate periodically positioned titanate quantum wires.⁸ The great advantage of zeolites in this capacity is their structural integrity, which may allow precise nanoscale 3D alignment of the quantum dots, nanoparticles, and clusters that now play central roles in nanoscience and nanotechnology. The idea has been realized with limited success, and a further effort is needed to achieve this goal.

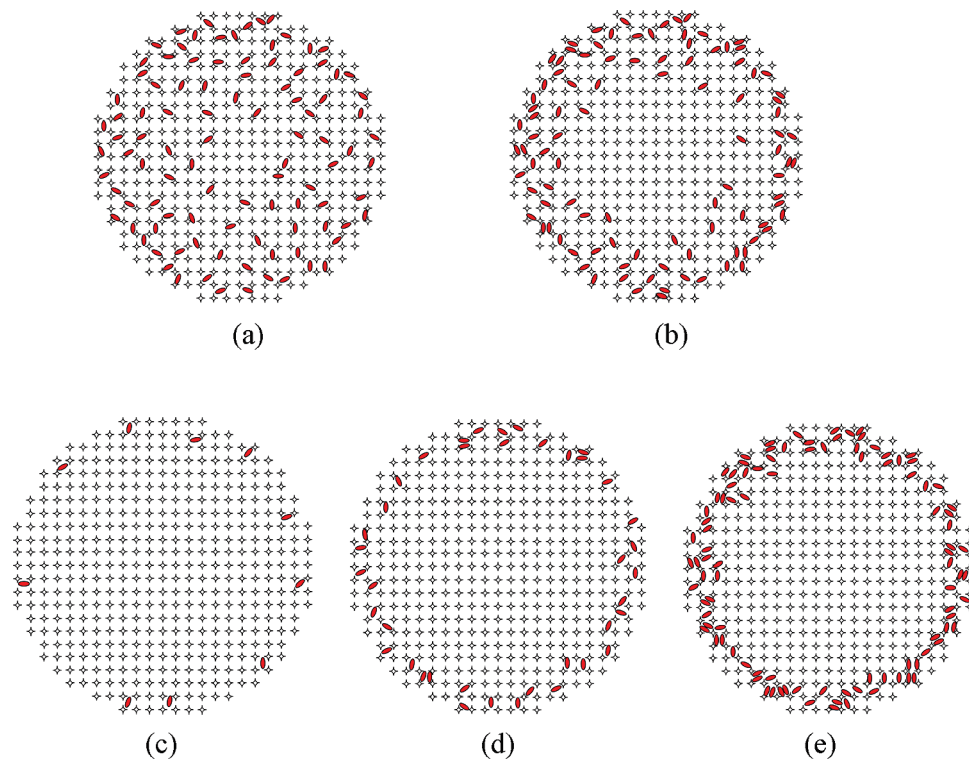
Zeolites are known to serve as support for guests not just within their cages/cavities and channels but also on their exterior surfaces. The spatial distribution of guests in and on a zeolite has heretofore been assumed to be homogeneous. In fact, however, distribution depends on the type of guest molecule and is often heterogeneous because of limited translational diffusion times (see Chart 1). Although heterogeneous distribution can be a drawback for homogeneous reaction–product formation, it can be an advantage for tracking a molecule within or between zeolite host crystals.

Chart 1 shows how the behavior of guest molecules in a host crystal depends on the size of the guest.⁹ Small molecules such as benzene and naphthalene diffuse into a host unperturbed and tend to equilibrate quickly (a). In contrast, large molecules such as perylene diffuse only with great difficulty and tend to get stuck near the surface of the host regardless of concentration (c,d). For this reason, observation of excimer emission upon photoexcitation becomes possible. Intermediate-sized molecules, anthracene and chrysene, fall somewhere in between

Received: November 20, 2010

Accepted: February 7, 2011

Published: February 15, 2011

Chart 1. Cross-Sectional Images of Zeolite Hosts That Are Embedded with Guest Molecules of Various Sizes and Amounts^a

^a(a) Small-size guest molecules, such as benzene or naphthalene, that can penetrate easily and quickly to achieve homogeneous distribution. (b) Intermediate-sized guest molecules, such as chrysene, that are somewhat hindered in their diffusional motion by the host's interconnecting windows and therefore penetrate more slowly. (c–e) Large-size guest molecules, such as perylene, that can be accommodated only on or near the host's surface because of their bulky size and for which molecular interactions such as dimer (excimer in the excited state) formation can be optimized by slightly increasing the loading level. (Modified from ref 9. Reproduced with permission from The Royal Society of Chemistry.)

regarding the mobility within zeolites (b). It takes time for these molecules to reach equilibrium (b → a). Thus, diffusion and distribution are important factors in photochemical reactions in zeolites.

Various types of spectroscopy are now used to study zeolite systems. Zeolite crystals are typically nanometer- to micrometer-sized and are normally treated as powders or suspensions for optimum synthetic yields and spectroscopic signal-to-noise ratios. Fluorescence spectroscopy has long proven useful for the study of solid systems because of the relative ease of signal acquisition, provided that scattering can be minimized. However, it was not until the development of the diffuse reflectance transient absorption spectroscopy¹⁰ that studies on the dynamics of nonfluorescent molecules and reaction intermediates, including radicals, radical ions, and triplet states, gained popularity in time domains ranging from femtoseconds through microseconds to milliseconds.¹¹ Relevant dynamics include the time-dependent evolution of configurational and conformational changes, translational motions, and chemical reactions at various time scales, and a knowledge of reaction dynamics is crucial to the understanding of mechanisms, particularly in complicated microheterogeneous systems such as zeolites.¹² The transient absorption spectroscopy has been a tool for intensive research in zeolite photochemistry. In-depth studies have been carried out for photoinduced electron transfer, electron trapping, and charge separation.^{13–20}

In addition, optical microscopy is emerging as an appropriate research tool with the advent of single-molecule spectroscopy²¹

and nanomaterials research.²² Various optical methods including confocal and dark-field techniques can be used to study zeolite systems. Micrometer- to millimeter-sized high-quality single crystals can be grown for zeolites that can include fluorescent dyes for use as targets in fluorescence microscopy,²³ commonly used in biological studies. Note, however, that the spatial resolution of a conventional optical microscope is fundamentally limited to about $\lambda/2NA$, where λ is the wavelength of the light used and NA is the numerical aperture of the objective. Thus, the spatial resolution of an optical microscope image is limited to ~200 nm for visible light, and the smaller details of, for example, zeolite cages and incorporated molecules cannot be resolved. To work within this limitation, one must either use very low concentrations of guest species to realize single-molecule conditions^{24,25} or make ensemble measurements.²⁶ We have worked mainly on the latter basis, using fluorescence microscopy to reveal slow dynamics. We have also used Rayleigh light-scattering spectroscopy coupled with dark-field microscopy²⁷ to investigate the distribution of gold nanoparticles within and among zeolite crystals. Importantly, we can use transient spectroscopy complementary with optical microscopy to reveal slow dynamics and distribution, given that the time scale of observation for the two methods differs; the former measures microseconds to milliseconds, and the latter measures greater than seconds.

A particularly intriguing application of transient absorption spectroscopy demonstrates intrazeolite intercage transport with zeolite powders adsorbed with two kinds of guest molecules.²⁸

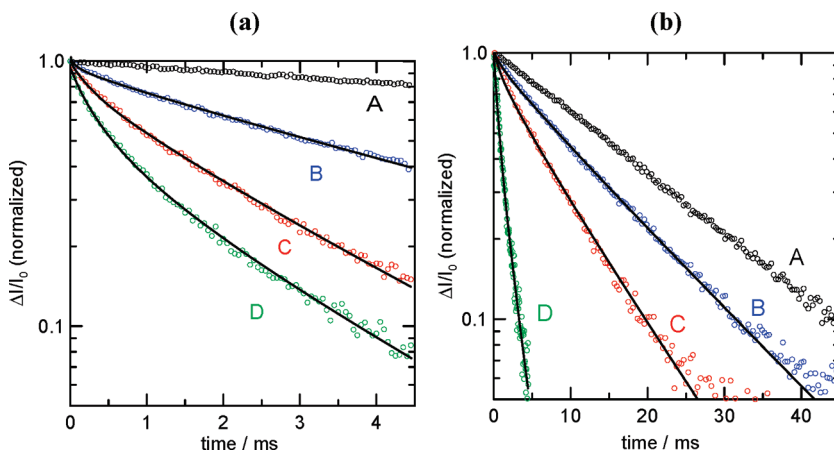


Figure 1. (a) Experimental decay curves of triplet-state anthracene in dehydrated zeolite Na⁺-Y at various azulene loading levels, (A) 0, (B) 7.6×10^{-6} , (C) 1.8×10^{-5} , and (D) 3.0×10^{-5} mol·g⁻¹. The loading level of anthracene was 5.0×10^{-6} mol·g⁻¹, the excitation wavelength was 355 nm (pulse width: 6 ns), and the monitoring wavelength was 420 nm. The ordinate represents the normalized absorption measured in diffuse reflectance mode. Absorption in the diffuse reflectance mode is defined as $\Delta I/I_0$ (where I_0 is the reflectance intensity before laser excitation and ΔI is the change in reflectance intensity after excitation), which is proportional to concentration when the values of $\Delta I/I_0$ are <10% (ref 10). The solid lines indicate fitting based on the CTRW model. The decay constant at low ($\leq 5.0 \times 10^{-6}$ mol·g⁻¹) loading levels was determined to be 54 ± 5 s⁻¹ when monitor light intensity was kept low so as not to heat the powdered samples. The mean occupancy numbers (average number of quenchers per supercage) of azulene are $\bar{n} = 0$ (A), 0.016 (B), 0.032 (C), and 0.18 (D). (b) Triplet-triplet absorption decay of anthracene in dehydrated Na⁺-Y zeolite, excited at 355 nm and monitored at 420 nm at various loading levels, (A) 5.0×10^{-6} , (B) 1.0×10^{-5} , (C) 2.0×10^{-5} , and (D) 1.1×10^{-4} mol·g⁻¹. The mean occupancy numbers are $\bar{n} = 0.008$ (A), 0.016 (B), 0.032 (C), and 0.18 (D). The self-decay rate constant is $k_0 = 35$ s⁻¹. (From ref 28. Reproduced with permission from The American Chemical Society.)

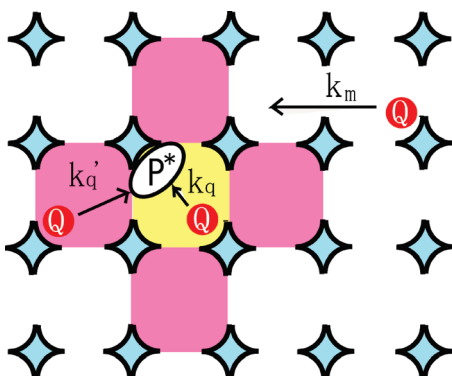


Figure 2. Quenching model for zeolite Na⁺-Y. P* represents a probe molecule (triplet donor), and Q represents a quencher molecule (triplet acceptor) that migrates within the cage network with a cage-to-cage jump rate constant of k_m . Two types of quenching mechanism are considered, (1) quenching within a cage, where the probe and quencher molecules are both present (quenching rate constant k_q), and (2) quenching in which the quencher molecules attack from the four direct neighboring cages (rate constant k'_q). Concentration-dependent quenching behavior is described by the mean occupancy number $\bar{n} = [\text{quencher}]/[\text{supercage}]$. (From ref 11. Reproduced with permission from Elsevier Inc.)

The kinetics of transients in zeolites is usually very different from the first- and second-order processes that govern most of solution chemistry. Figure 1 shows the quenching of photoexcited triplet-state anthracene by triplet-triplet energy transfer for various quantities of the energy-acceptor azulene (a) and anthracene itself (b), both adsorbed in Na⁺-exchanged zeolite Y, referred to as Na⁺-Y.

At sufficiently low loading levels of the quencher azulene, the decay of triplet-state anthracene is approximated by a single exponential function, consistent with first-order self-deactivation

in the absence of a quencher. At increasing concentrations of quencher, dynamic quenching of triplet-state anthracene is observed; the decay rate increases (nonexponentially) with increasing loading level of quencher. The probe molecule, anthracene, is expected to either self-deactivate or undergo quenching by collision with another doped species, a quencher, continuously migrating within the cage networks because triplet-triplet energy transfer proceeds by collisions and involves the exchange mechanism. Quenching behavior similar to that of azulene was observed for the self-quenching of the triplet-state anthracene (Figure 1b).

The kinetics of excited-state quenching in zeolites is conveniently described in terms of the continuous time random walk (CTRW) model.²⁸ The model assumes that quenchers perform independent random walks that involve unbiased jumps to the four nearest-neighbor supercages and that the waiting time distribution function for each supercage is exponential. Supercages are assumed to be randomly occupied by reactants according to Poisson's law. For open zeolite structures, quenching may also occur when the probe and the quencher reside in direct neighboring supercages. The essential points of the model are illustrated schematically in Figure 2.

Two significant findings were obtained from this triplet quenching study. First, self-diffusion coefficients were extracted from the cage-to-cage migration rate constant k_m for anthracene and azulene in dehydrated Na⁺-Y. The observed very small values, 10^{-15} – 10^{-16} m²·s⁻¹ at room temperature, cannot be measured by the traditional techniques of pulsed field gradient NMR and quasielastic neutron scattering that have been used to measure the self-diffusion coefficient of benzene in Na⁺-Y (10^{-10} – 10^{-13} m²·s⁻¹ at 298 K). Thus, triplet quenching, which probes longer (milliseconds to several hundreds of milliseconds) time scales, depending on the triplet lifetime, is complementary

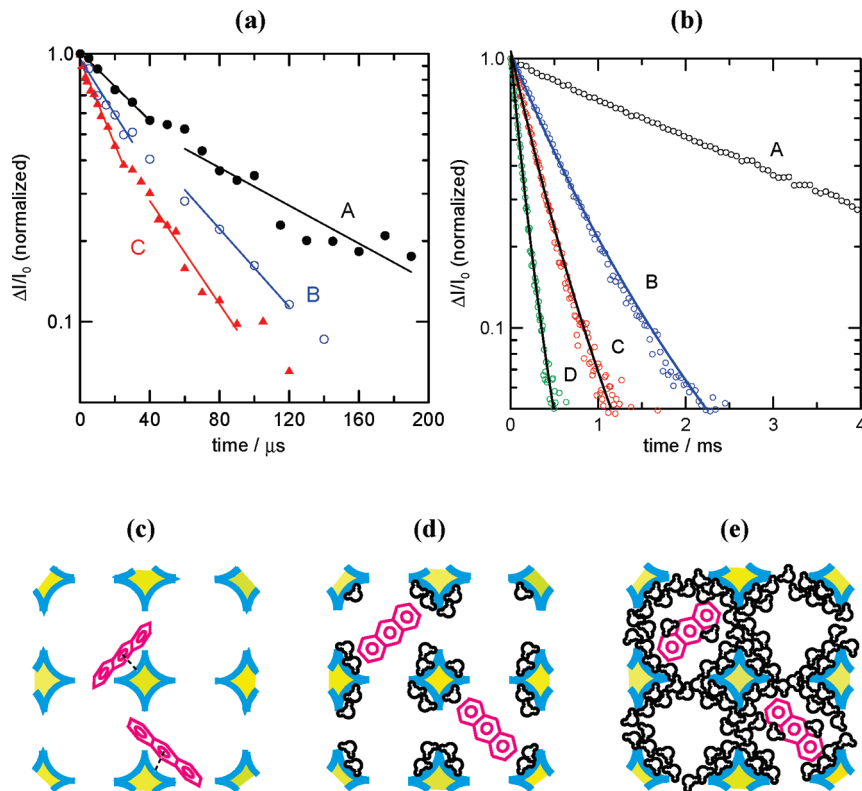


Figure 3. (a) Decay curves of triplet-state anthracene in $0.10 \text{ cm}^3 \cdot \text{g}^{-1}$ hydrated $\text{Na}^+ - \text{Y}$ at constant laser intensities and various anthracene loading levels, (A) 1.0×10^{-6} , (B) 5.0×10^{-6} , and (C) $1.0 \times 10^{-5} \text{ mol} \cdot \text{g}^{-1}$. Decay is remarkably fast because of self-quenching caused by enhanced mobility resulting from hydration. (b) Triplet-triplet absorption decay curves of anthracene in $0.26 \text{ cm}^3 \cdot \text{g}^{-1}$ hydrated zeolite $\text{Na}^+ - \text{Y}$, excited at 355 nm and monitored at 420 nm at various anthracene loading levels, (A) 1.0×10^{-6} , (B) 2.0×10^{-5} , (C) 4.5×10^{-5} , and (D) $1.1 \times 10^{-4} \text{ mol} \cdot \text{g}^{-1}$. At increased but still less than full hydration, decay slows down because of decreased concentration quenching due to decreased mobility. The mean occupancy numbers are $\bar{n} = 0.018$ (A), 0.032 (B), 0.071 (C), and 0.18 (D). (c–e) Pictorial representation of anthracene molecules in zeolite $\text{Na}^+ - \text{Y}$ at various degrees of hydration; (c) dehydrated zeolite $\text{Na}^+ - \text{Y}$, (d) $0.05 - 0.1 \text{ cm}^3 \cdot \text{g}^{-1}$ hydrated $\text{Na}^+ - \text{Y}$, and (e) $0.2 - 0.3 \text{ cm}^3 \cdot \text{g}^{-1}$ hydrated $\text{Na}^+ - \text{Y}$. (From refs 28 and 30. Reproduced with permission from The American Chemical Society.)

to other established techniques.²⁹ Second, analysis of the experimental decay curves, based on the CTRW model, reveals that the reaction mechanism depends on the zeolite lattice topology as well as the dynamics of guest molecule migration between adsorption sites. In dehydrated $\text{Na}^+ - \text{Y}$ zeolite, where connecting windows are open so that molecular access is easy and the distance between adsorption sites in neighboring cages is small enough to allow sufficient overlap of the wave functions, probes can be deactivated by quenchers that reside not only in the same cage but also in the four cages of the first coordination sphere (see Figure 2).

In this context, the remarkable effect of coadsorbed solvent molecules, especially water, on guest diffusivity deserves comment.³⁰ Figure 3 shows an example of this effect on the diffusivity of anthracene, measured by triplet quenching. Here, a weighed amount of water was introduced through a vacuum line into an optical cell containing dry zeolite powder (also weighed) and sealed afterward.

Consider the decay curves at three low levels of hydrated $\text{Na}^+ - \text{Y}$ (Figure 3a). For partial ($0.05 - 0.10 \text{ cm}^3 \cdot \text{g}^{-1}$) as compared to full ($0.378 \text{ cm}^3 \cdot \text{g}^{-1}$) hydration, the decay rate of triplet-triplet absorption is about 1000 times faster for a loading level of $1.0 \times 10^{-5} \text{ mol} \cdot \text{g}^{-1}$ (see the difference between Figure 3a and Figure 1b, which shows a dehydrated system). This is because the greatly increased mobility caused by hydration enhances self-quenching, that is, quenching of triplet-state

anthracene by ground-state anthracene. In dehydrated zeolites, aromatic species are held strongly to the cationic sites within the supercages (Figure 3c), and the deactivation rate of the triplet state is very low because of the absence of quenching. Adsorption of critical amounts of water molecules can enhance diffusional motion by liberating the molecules from the zeolite frameworks (Figure 3d). Cation- π interaction is known to be responsible for such interaction.³¹ In contrast, a large ($0.2 - 0.3 \text{ cm}^3 \cdot \text{g}^{-1}$) quantity of water can greatly reduce guest mobility by interfering with diffusional motion, for instance, by blocking interconnecting windows between cages (Figure 3e). This situation slows down the deactivation rate of triplet-state anthracene again but not to the level of a dehydrated system (Figure 3b).

Thus, the dynamic behavior of a guest aromatic molecule within a zeolite is critically dependent on the balance of interactions among zeolite frameworks, guest species, and coadsorbed water. In particular, coadsorbed water can control the intrazeolite motion of the guest species. Alternatively, measurements of triplet decay time or mobility within a zeolite can be used to monitor the degree of hydration. In addition to water, other polar molecules such as acetonitrile, methanol, and pyridine play an important role in enhancing and interfering with the motion of a guest, but *n*-hexane does not. In nearly fully hydrated $\text{Na}^+ - \text{Y}$, plain aromatic molecules such as anthracene, phenanthrene, and chrysene are excluded from interior void spaces but crystallize on

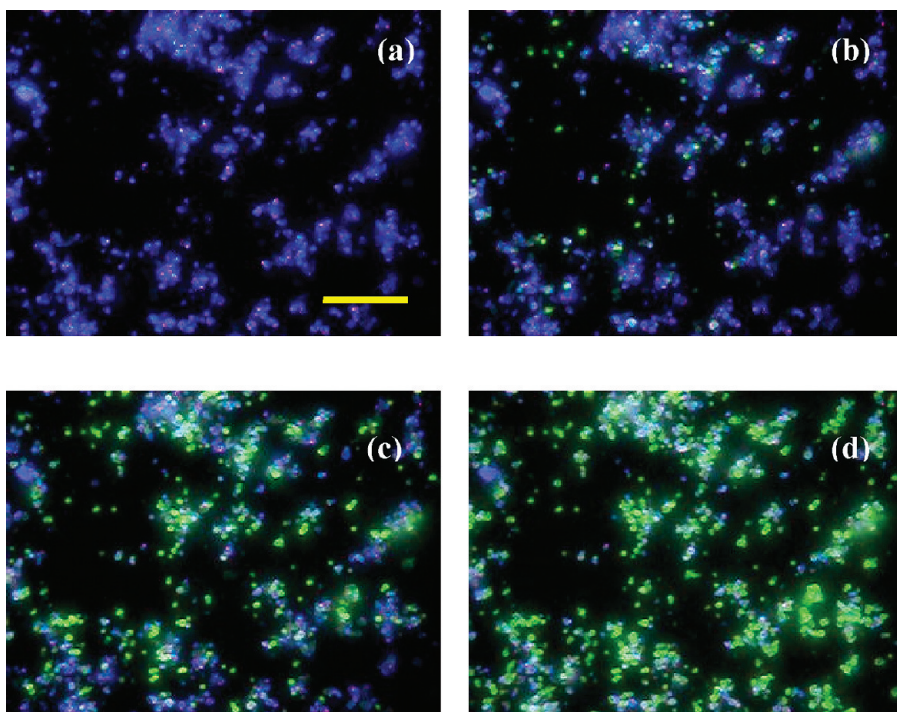


Figure 4. Fluorescence image (excitation wavelength: 330–385 nm) of zeolite $\text{Ti}^+ - \text{X}$ crystals loaded with $1.0 \times 10^{-5} \text{ mol} \cdot \text{g}^{-1}$ chrysene (chrysene/ $\text{Ti}^+ - \text{X}$) during heating with a heat gun for various times, (a) 0, (b) 15, (c) 30, and (d) 50 s. Initially, the zeolite crystals are hydrated, inducing fluorescence emission of chrysene; with heating, dehydration of the host zeolite proceeds, inducing phosphorescence emission of chrysene because of increased interaction with the charge-compensating cation Ti^+ . Dehydration–hydration cycles are completely reversible. The scale bar represents 50 μm .

the exterior surface of the crystal, as deduced from fluorescence spectra.³¹

The dynamic behavior of a guest aromatic molecule within a zeolite is critically dependent on the balance of interactions among zeolite frameworks, guest species, and coadsorbed water.

Interestingly, pumping out the water molecules from a zeolite crystal's interior enables the guest molecules to go back inside of the crystal. This reversible crystallization–dissolution process, which is dependent on hydration level, can be monitored by fluorescence spectroscopy or microscopy. The microscopy approach is simple and appealing to the eye by providing real-time positional information. Microscopy observations of chrysene in Ti^+ -exchanged zeolite X ($\text{Ti}^+ - \text{X}$) are shown in Figure 4.

In the figure, at first, we observe blue fluorescence emission from the crystals because the environment surrounding chrysene is hydrated, similar to that shown in Figure 3e, and interaction of the guest with the charge-compensating cation is weak. With heating, the environment becomes increasingly dehydrated, to a state similar to that shown in Figure 3c, allowing development of cation– π interaction for chrysene. Because of the strong inter-system crossing enhancement effect of Ti^+ , with time, we

observe green phosphorescence emission from the crystals. Importantly, the observed fluorescence–phosphorescence interconversion is reversible. It is also interesting to note that the important role of trace water in the nonuniform functionalization of 1D mesoporous silica channels with alkoxy silanes was visualized with confocal fluorescence microscopy by another group.³²

To summarize thus far, we have briefly described how intracrystalline diffusivity is measured spectroscopically based on slow-quenching kinetics originating from triplet–triplet absorption decay. This method is applicable to the long-lived transient absorption of reactive intermediates such as radicals and radical ions and also to the phosphorescence–emission decay of various molecules. The method enables us to obtain, for the first time, cage-to-cage diffusion coefficients in zeolites for various species. Quenching kinetics depends also on framework structure. An attractive area for future investigation is comparison of molecular diffusivities in 3D cage network structures with those in 1D channel structures as these data would definitely contribute to a thorough understanding of chemical reactions in zeolites. This and related efforts are needed to determine as-yet-unexplored diffusivities of various guest species that are dependent on the guest molecule, host framework structure, and mutual interaction.

Microscopy is particularly suitable for visualizing the spatial distribution and resultant chemical reactions in the restricted space of a single zeolite crystal.³³ Figure 5 shows two experiments investigating intercrystalline migration of emissive guest molecules between crystals in contact and the resultant photochemistry.

Figure 5A shows the movement of chrysene molecules from zeolite $\text{Na}^+ - \text{X}$ to $\text{Ti}^+ - \text{X}$ crystals. A group of $\text{Na}^+ - \text{X}$ crystals

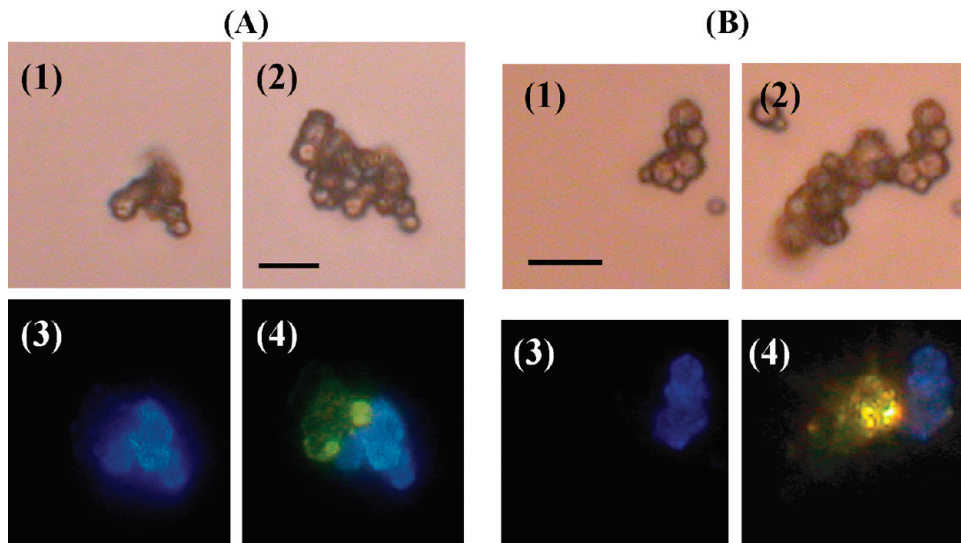


Figure 5. (A) Microscopy images of a system of one guest species and two groups of zeolite crystals. (1) and (2) are bright-field images; (3) and (4) show the time evolution of fluorescence (excitation wavelength: 330–385 nm). (1) Zeolite Na⁺—X particles incorporated with 1.0×10^{-5} mol·g⁻¹ chrysene; (2) the same zeolite Na⁺—X as in (1) in contact with unloaded Ti⁺—X particles added later; (3) fluorescence image of (2) just after preparation, showing only fluorescence from chrysene/Na⁺—X; (4) fluorescence image of (2) 60 min after preparation, showing green emission from Ti⁺—X with distance-dependent intensity. Observations were made with dehydrated zeolites. The scale bar represents 10 μ m. (B) Microscopy images of a system of two guest species. (1) and (2) are images in transmittance mode; (3) and (4) are images in fluorescence mode. (1) Zeolite Na⁺—X particles incorporated with 1.0×10^{-5} mol·g⁻¹ chrysene (chrysene/Na⁺—X); (2) the same zeolite Na⁺—X as in (1) with 4.0×10^{-5} mol·g⁻¹ TCNB (TCNB/Na⁺—X) particles added later; (3) fluorescence image (excitation wavelength: 330–385 nm) of (2) just after preparation, showing only blue fluorescence from chrysene/Na⁺—X; (4) fluorescence image of (2) 60 min after preparation, showing yellow emission from TCNB/Na⁺—X with distance- and time-dependent intensity. The scale bar represents 10 μ m. (From ref 33. Reproduced with permission from Wiley—VCH.)

loaded with chrysene is mounted on a coverslip; then, a group of unloaded (empty) Ti⁺—X crystals is added to act as a molecular trap. We observe blue fluorescence emission only from Na⁺—X, followed by green phosphorescence emission from Ti⁺—X. The latter, enforced by the intersystem crossing enhancement effect of the charge-compensating cations, indicates the inclusion of chrysene into Ti⁺—X. The emission intensity clearly decreases with increasing distance, suggesting that chrysene migration occurs as a result of diffusional motion with a time scale of minutes to several tens of minutes at ambient temperature. In this example, molecular migration is indicated by the presence of a luminescence color that is characteristic of a particular zeolite crystal and originates from the specific photochemistry of the adsorbed species. Although qualitative, real-time changing images can be captured during molecular migration.

Figure 5B shows the migration-assisted formation of a charge-transfer (CT) complex between electron-donating chrysene and electron-accepting 1,2,4,5-tetracyanobenzene (TCNB). The CT complex of two guest species in zeolite is known to originate from the strong molecular confinement effect exerted by the host.^{34,35} The peak position of the CT bands suffers an appreciable blue shift depending on the electron-donating properties of zeolite hosts originating from cation exchange. Additionally, the equilibrium constant of CT complex formation depends on the electron-donating–accepting property of the zeolite host and also on aromatic donor molecules. On the basis of these observations, the driving force of the complex formation was ascribed to a strong electron-accepting property of the TCNB—zeolite host complex, which attracts arene donors.³⁴ Importantly, the fluorescence microscopy method gives a space-resolved picture of the reaction. Here, two groups of Na⁺—X crystals, one

containing the donor chrysene and one containing the acceptor TCNB, are placed side-by-side on a coverslip, in the order listed. We observe fluorescence emission from chrysene, followed gradually by yellowish emission from TCNB/Na⁺—X, ascribable to the CT complex of chrysene and TCNB. The emission intensity decreases with increasing distance between the borders of chrysene / Na⁺—X and TCNB/Na⁺—X. Interestingly, the initial stages of CT complex formation seem to be governed by migration of chrysene, not that of TCNB. Later, we observe very weak CT emission from the crystals originally incorporated with chrysene.

It should be emphasized that the driving force of guest migration between two loaded crystals is primarily CT interaction; without such a driving force, migration is not feasible. In contrast, the driving force of guest migration from a loaded crystal to an unloaded crystal is primarily the activation energy of transfer, which is approximately correlated with the binding strength between the molecule and the zeolite host, measured by temperature-programmed desorption (TPD). This difference is evident in a comparison of phenanthrene/Na⁺—Y with phenanthrene/Ti⁺—Y. Basically, the binding strength of a guest species is strongly dependent on the charge-compensating cations with which it undergoes cation– π interaction. TPD results show that the desorption temperature of phenanthrene is higher when it is adsorbed in Ti⁺—Y rather than in Na⁺—Y, suggesting that the binding strength is higher for Ti⁺—Y than that for Na⁺—Y.³⁶ This observation is consistent with the experimental results for guest migration from Na⁺—X to Ti⁺—X described above. Meanwhile, the migration in the reverse direction, from Ti⁺—X to Na⁺—X, was not observed. We observed the same general trend for plain aromatics, including anthracene and chrysene. Note that we did not clearly observe guest migration between crystals of the same type,

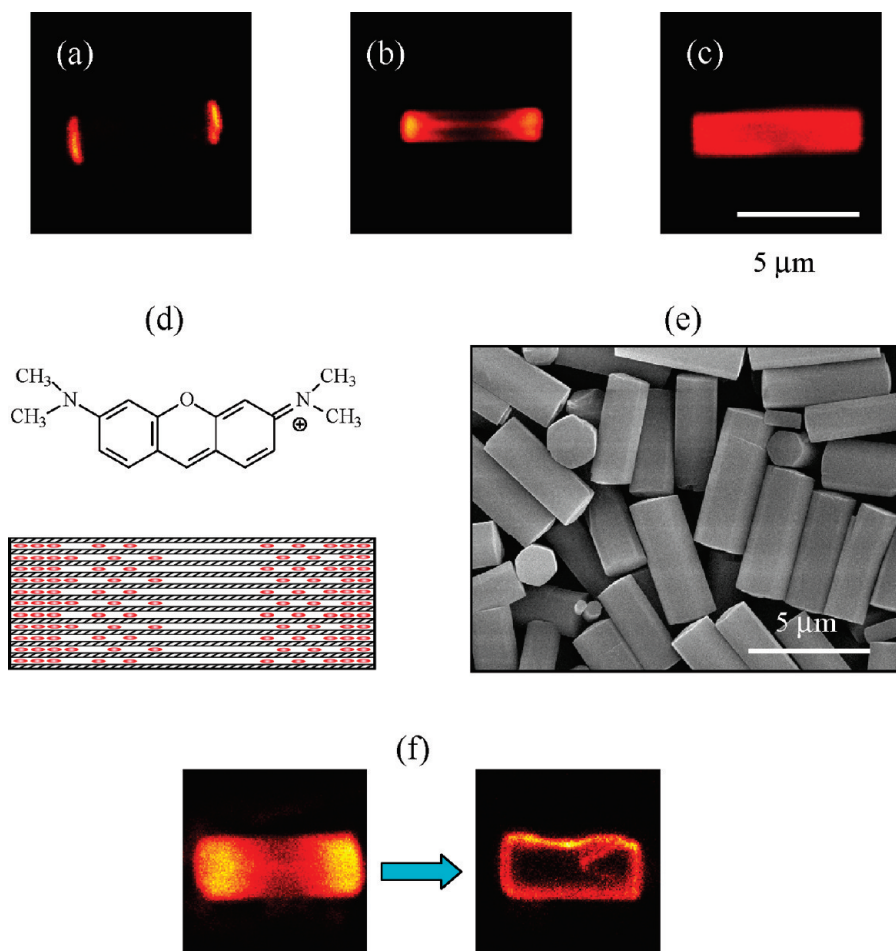


Figure 6. Microscopy and SEM images of zeolite L crystals. (a–c) Cross-sectional images (false color image) obtained by confocal microscopy for zeolite L incorporated with $1.4 \times 10^{-5} \text{ mol} \cdot \text{g}^{-1}$ pyronine Y at various conditions of preparation in aqueous solution, (a) 48 h of agitation at room temperature, (b) 48 h of agitation at 85 °C, and (c) 96 h of agitation at 85 °C. (d) Structural formula of cationic dye pyronine Y and pictorial representation of dye penetration inside of 1D channels running along the cylindrical-shaped L crystals. (e) SEM image of cylindrical-shaped zeolite L crystals. (f) Confocal microscope image representing the dye exit replaced by water. (Modified from ref 37. Reproduced with permission from Elsevier Inc.)

suggesting that different binding strengths might be necessary to induce migration.

These microscopy results for intercrystalline migration and migration-assisted photochemical reactions are rather qualitative. An attractive area for future investigation is quantification of distance- and time-dependent emission intensities in terms of rate constants or intercrystalline diffusion coefficients as this type of work would help us understand the kinetics of intercrystalline migration of guest species. This will require a more sophisticated technique that can manipulate two single zeolite crystals to place with any desired geometry. Improved spatial resolution can be achieved by use of confocal microscopy. Such efforts are vital.

During the course of our microscopy investigation of zeolites, we observed various fluorescence intensities that were dependent on the statistical distribution of guest molecules to the individual crystals.⁹ An example is bulky perylene, whose size is close to the pore size of the host $\text{Na}^+ - \text{X}$ and whose adsorption rate is therefore slow. In this case, crystal-to-crystal variations occur in the guest molecule loading level, as shown in Chart 1c–e. A Gaussian-type histogram describes the crystal-to-crystal variations in fluorescence intensity, suggesting that the concentration of adsorbed molecules for each crystal is not the same but depends in a statistical manner on the individual crystals. These

variations in crystal-to-crystal loading give rise not only to fluorescence intensity but also to crystal-dependent excimer emission of perylene highly loaded in $\text{Na}^+ - \text{X}$.⁹

The spatial distribution of molecules within a single zeolite crystal can be actually heterogeneous, as revealed by confocal microscopy.³⁷ Figure 6 shows the adsorption of the cationic fluorescent dye pyronine Y into a channel-type zeolite L ($\text{K}^+ - \text{L}$) crystal.

Fluorescence images were taken during adsorption. At first (Figure 6a), the dye molecules (the structural formula and internal channel structure are shown in Figure 6d) reside only at the ends of the cylindrical zeolite crystal (crystal image shown in Figure 6e). With time, the dye molecules gradually penetrate the crystal's channels, which are straight and open only at the ends. Clearly, achieving homogeneous distribution throughout the crystal requires time for complete diffusion. Note that the confocal fluorescence images can show not only the progress of the dye inclusion but also the exclusion of the dyes, which are replaced by water molecules from inside to outer surfaces (Figure 6f), as described above for hydrophobic neutral guests.

The likelihood of intrazeolite and interzeolite spatially inhomogeneous loading of externally introduced guest molecules prompted us to count the incorporated species and determine

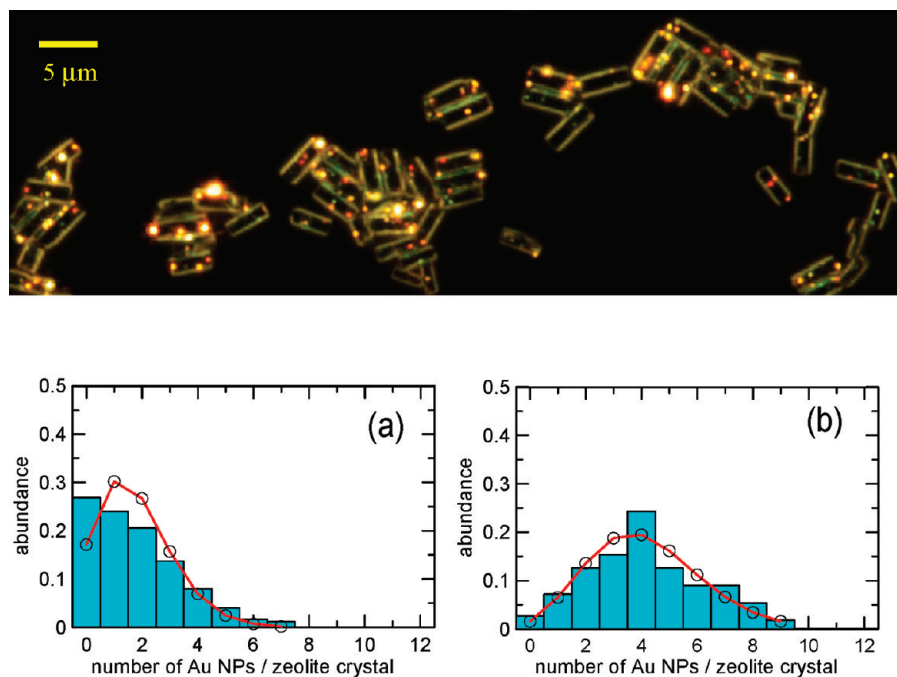


Figure 7. Upper panel: dark-field light-scattering images of Au NP-doped zeolite L crystals. Lower panel: plots of the number of Au NPs per zeolite crystal (occupancy) versus abundance for different quantities of Au NPs in zeolite crystals. Bar charts show experimental results for approximately 200 zeolite crystals; line plots show calculated curves based on a Poisson distribution for various experimental average occupancies, (a) 1.8 and (b) 4.2. (Modified from ref 38. Reproduced with permission from The American Chemical Society.)

the statistical distribution of zeolite inclusion. For this purpose, we investigated the inclusion of gold nanoparticles (Au NPs) during zeolite synthesis.³⁸ Because of their extremely intense light-scattering capability in the visible region induced by localized surface plasmon resonance (LSPR), spherical Au NPs of diameter >40 nm can easily be detected by conventional dark-field microscopy as diffraction-limited spots.²⁷

Figure 7a shows a white-light-scattering image of zeolite L crystals embedded with Au NPs. Various NP colors, such as green, yellow, and red, indicate the presence of various-sized Au NPs as the peak positions in the scattering spectra are characteristic of the particle diameter. Particle size depends on the preparation method, and our chosen method was laser ablation synthesis, which enables preparation of Au colloids that are stable in a zeolite synthetic gel. Figure 7b and c shows histograms of the number of Au NPs per zeolite crystal, equivalent to occupancy as determined by inspection of the light-scattering images of individual crystals. The average occupancies for the two figures are 1.8 and 4.2, respectively, and the distribution function is well fitted by a Poisson statistical distribution. A Poisson distribution has previously been observed for guest inclusions in micelles and microemulsions, particularly at low loading levels, and has thus been established as a guiding principle for molecular inclusion.³⁹ Here, we have experimentally demonstrated that the interzeolite distribution statistics are a Poisson distribution, which can be a good measure for predicting how molecules can distribute themselves among zeolite crystals at low levels of loading. Unfortunately, because of agglomeration during the synthesis, the Au NPs are too big to be incorporated into the channels of zeolite L crystals. Thus, the present result can be regarded as a demonstration offering a simple method of imaging without resorting to transmission electron microscopy (TEM).

To increase the spatial resolution of a detection system, use of confocal light-scattering microscopy exploiting a femtosecond supercontinuum as a light source is appropriate. This method can display the 3D scattering image of Au NPs included in a single crystal and can detect Au NPs with diameters as small as 10 nm. Spectral measurement of individual NPs should enable determination of particle size, particle aggregation, intracrystalline distribution, and concentration of NPs per crystal. Figure 8 shows a single octahedral zeolite Na^+ -Y crystal of approximately 8 μm .

The upper part of the figure shows slice images (taken in 1- μm steps); the colored spots correspond to Au NPs, and incorporation of Au NPs inside of the crystal is evident. The lower part of the figure shows the light-scattering spectra of individual Au NPs, the scattered light which was isolated with a pinhole. Spectra A, B, and C originate from a single Au NP; D originates from aggregated NPs. Thus, dark-field microscopy—spectroscopy is promising for characterizing the noble metal particles Au and Ag embedded in host materials. Moreover, the combination of dark-field and fluorescence microscopy—spectroscopy has potential to reveal the catalytic reactions⁴⁰ and plasmon-enhanced photochemistry⁴¹ of guest species in Au-NP-loaded zeolites.

The microscopy approach has attracted widespread interest of zeolite photochemists. Studies with various aspects have been carried out. For instance, molecules with adequate size and shape can enter in one-dimensional channel-type zeolites $\text{AlPO}_4\text{-5}$ and L, with a preferential direction enforced by the geometric restrictions that align the chromophores. The orientation of the molecules with respect to the *c*-axis of the host crystals was visualized for single crystals by optical or fluorescence microscopy using polarization radiation.^{42–44} Leakage of dye molecules is often observed when incorporated into zeolite crystals that were dispersed in water or exposed under physiological conditions. For preventing the dye leakage, techniques exploiting

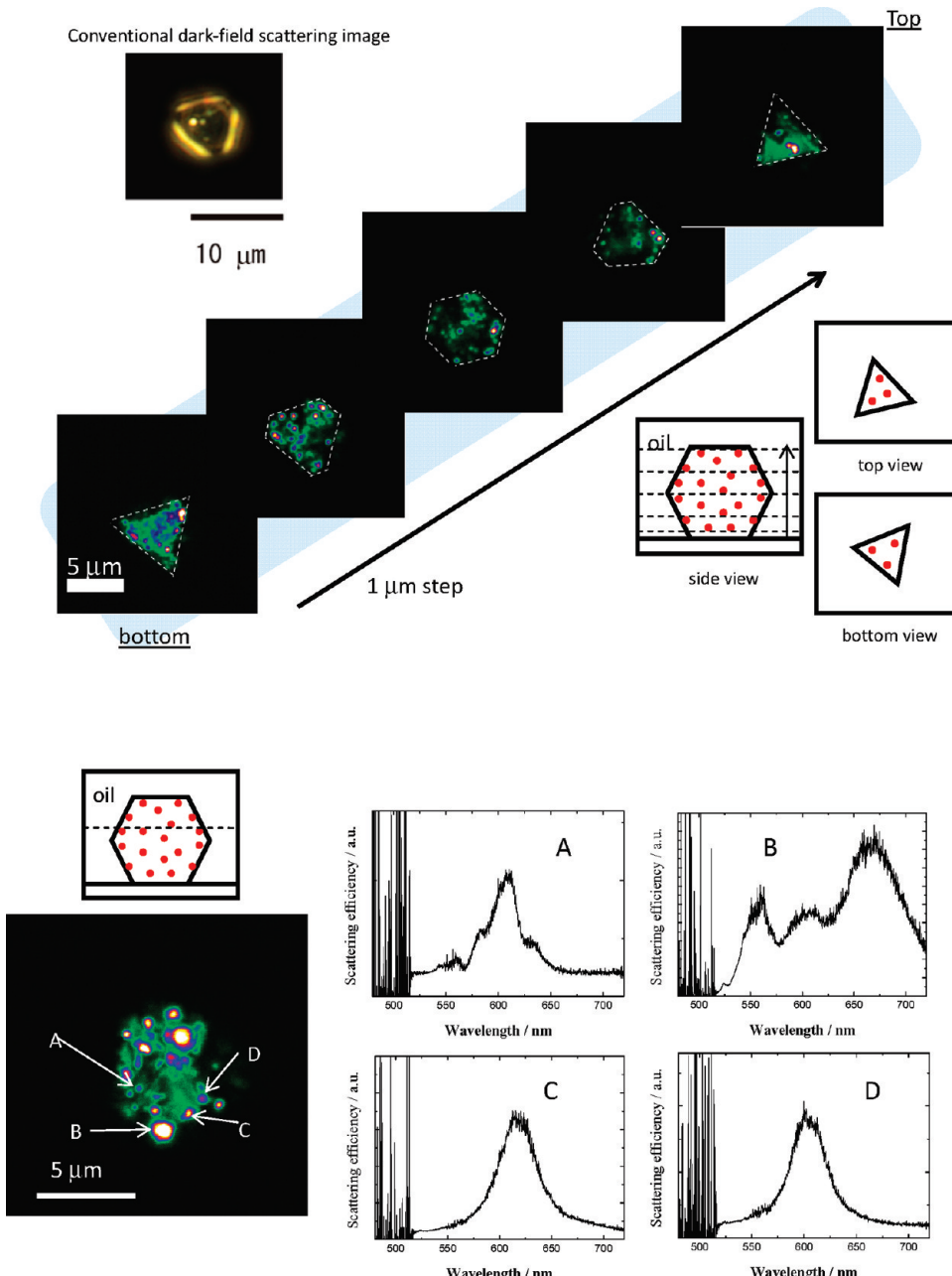


Figure 8. 3D light-scattering images of Au NPs in a single crystal of zeolite $\text{Na}^+ - \text{Y}$ ($8 \mu\text{m}$), obtained by confocal light-scattering microscopy exploiting a femtosecond supercontinuum as a scattering light source. Upper panel: conventional and confocal light-scattering images; the confocal slice images were acquired in $1\text{-}\mu\text{m}$ steps. Lower panel: white light-scattering spectra of individual Au NPs; spectra A, B, and C are from a single Au NP, and D is from aggregated NPs.

silica coating and stopcock molecules have been found effective by direct microscopy observation.^{45,46} Multicolor photoluminescent silver clusters were characterized within cation-exchanged and thermally treated zeolite matrixes to a single-crystal level.⁴⁷ The fluorescence microscopy is the most useful to unravel internal structure and pore accessibility for ZMS-5 crystals that have applications as a shape-selective catalyst.^{48–50} Microscopy can be used to acquire new insight into the catalytic activity of working microporous crystalline materials. When tools with high spatial resolution are employed, unexpected details of pore organization and product location will be revealed.

Since the beginning of this century, the application of zeolites to advanced materials, including lasers, LEDs, and solar cells, has been actively investigated,²³ and a method has been developed to achieve 2D and 3D organization of zeolite microcrystals for device fabrication.⁵¹ Increasing demand exists for a method that can characterize the basic properties of zeolite composite materials such as luminescence and electron transport for photonic applications. The two experimental techniques discussed in this report, diffuse reflectance transient absorption spectroscopy and confocal optical microscopy, are complementary and well-suited for characterization of the electronic and photonic properties of either large-area or single crystals. To apply these

characterization methods to their maximum capability, extra effort should be devoted to develop new zeolite composite materials. A few promising examples have been reported to date. Observation of room-temperature phosphorescence⁵² in various aromatic species tightly fitted into the narrow channels of a host suggests that triplet excited states that usually deactivate via various pathways can gain extended lifetimes because of significantly reduced nonradiative processes when the species is rigidly held. Potential generation of triplet carbenes⁵³ and triplet excimers⁵⁴ at room temperature also shows that inclusion can stabilize reactive intermediates. These results suggest that zeolites can be useful as containers for preserving important but unstable chemicals such as pharmaceuticals. Furthermore, zeolites can contribute to nanomaterials research by including quantum dots so as to prevent unfavorable blinking (intermittence in emission) phenomena and also by including gold nanorods oriented parallel along the channel direction so as to act as an anisotropic material. Material innovations and development of further new spectroscopic characterization methods should revitalize zeolite photochemistry in the 21st century.

Material innovations and development of further new spectroscopic characterization methods should revitalize zeolite photochemistry in the 21st century.

AUTHOR INFORMATION

Corresponding Author

*E-mail: hashi@eco.tokushima-u.ac.jp

BIOGRAPHY

Shuichi Hashimoto is a Professor of Ecosystem Engineering, The University of Tokushima. He earned a Ph.D. in physical chemistry from Tokyo Metropolitan University and performed postdoctoral research at the University of Notre Dame. His current research interests are the optical microscopy study of zeolite photochemistry, pulsed laser-induced transformations of noble metal nanoparticles, and microscopy—spectroscopy of nanoparticles and nanostructures.

ACKNOWLEDGMENT

This work was supported in part by Grants-in-Aid for Scientific Research (No. 21020025, on “Priority Area on Strong Photon-Molecule Coupling Field (No. 470)” and No. 2265-5043) and by the Tokyo Ohka Foundation for the Promotion of Science and Technology (Research Grant 2010). T. Uwada is acknowledged for help with dark-field microscopy—spectroscopy measurements.

REFERENCES

- (1) van Bekkum, H.; Flanigen, E. M.; Jacobs, P. A.; Jansen, J. C., Eds.; *Introduction to Zeolite Science and Practice*; Elsevier: Amsterdam, The Netherlands, 2001.
- (2) Steed, J. W.; Atwood, J. L. *Supramolecular Chemistry*, 2nd ed.; Wiley: Chichester, U.K., 2009.
- (3) Turro, N. J.; Ramamurthy, V.; Scaiano, J. C. *Modern Molecular Photochemistry of Organic Molecules*; University Science Books: Sausalito, CA, 2010; pp 925–1000.
- (4) Ramamurthy, V.; Schanze, K. Eds. *Solid State and Surface Photochemistry*; Marcel Dekker: New York, 2000.
- (5) Corma, A.; Garcia, H. Zeolite-based Photocatalysts. *Chem. Commun.* **2004**, 1443–1459.
- (6) Ozin, G. A.; Arsenault, A. C.; Cademartiri, L. *Nanochemistry*, 2nd ed.; Royal Society of Chemistry: London, 2009.
- (7) Jeong, N. C.; Kim, H. S.; Yoon, K. B. New Insight into CdS Quantum Dots in Zeolite—*J. Phys. Chem. C* **2007**, *111*, 10298–10312.
- (8) Jeong, N. C.; Lee, Y. J.; Park, J.-H.; Lim, H.; Shin, C.-H.; Cheong, H.; Yoon, K. B. New Insights into ETS-10 and Titanate Quantum Wire: A Comprehensive Characterization. *J. Am. Chem. Soc.* **2009**, *131*, 13080–13092.
- (9) Hashimoto, S.; Uehara, K.; M. Sogawa, K.; Takada, H.; Fukumura, H. Application of Time- and Space-Resolved Fluorescence Spectroscopy to the Distribution of Guest Species into Micrometer-Sized Zeolite Crystals. *Phys. Chem. Chem. Phys.* **2006**, *8*, 1451–1458.
- (10) Wilkinson, F.; Kelly, G. In Scaiano, J. C., Ed. *Handbook of Organic Photochemistry*; CRC Press: Boca Raton, FL, 1989; Vol. 1, pp 293–326.
- (11) Hashimoto, S. Zeolite Photochemistry: Impact of Zeolites on Photochemistry and Feedback from Photochemistry to Zeolite Science. *J. Photochem. Photobiol. C* **2003**, *4*, 19–49.
- (12) Gil, M.; Ziolek, M.; Organero, J. A.; Douhal, A. Confined Fanst and Ultrafast Dynamics of a Photochromic Proton-Transfer Dye within a Zeolite Nanocage. *J. Phys. Chem. C* **2010**, *114*, 9554–9562.
- (13) Gener, I.; Bunitinx, G.; Moissette, A.; Bremard, C. Photochemistry of Biphenyl Occluded within X Faujasite Type Zeolites. *J. Phys. Chem. B* **2002**, *106*, 10322–10329.
- (14) Ellison, E. H. Influence of Oxygen on the UV-Photocatalyzed Generation of Pyrene Cation Radicals in the Zeolites X and Y. *J. Phys. Chem. B* **2004**, *108*, 4607–4618.
- (15) Ellison, E. H. Electron Trapping in Polar-Solvated Zeolites. *J. Phys. Chem. B* **2005**, *109*, 20424–20432.
- (16) Ellison, E. H. Adsorption and Photophysics of Fullerene C₆₀ at Liquid–Zeolite Particle Interfaces: Unusually High Affinity for Hydrophobic, Ultrastabilized Zeolite Y. *J. Phys. Chem. B* **2006**, *110*, 11406–11414.
- (17) Alvaro, M.; Chretien, M. N.; Fornes, V.; Galletero, M. S.; Garcia, H.; Scaiano, J. C. Multicomponent Donor–Acceptor Relay System Assembled within the Cavities of Zeolite Y. Photoinduced Electron Transfer between Ru(bpy)₃²⁺ and 2,4,6-Triphenylpyrilium in the Presence of Interposed TiO₂. *J. Phys. Chem. B* **2004**, *108*, 16621–16625.
- (18) Alvaro, M.; Corma, A.; Ferrer, B.; Garcia, H.; Palomares, E. Laser Flash Photolysis Study of Anthracene/Viologen Charge Transfer Complex in Non-Polar, Dealuminated Zeolites. *Phys. Chem. Chem. Phys.* **2004**, *6*, 1345–1349.
- (19) Atienzar, P.; Corma, A.; Garcia, H.; Scaiano, J. C. Diffuse Reflectance Laser Flash Photolysis Study of Titanium-Containing Zeolites. *Chem. Mater.* **2004**, *16*, 982–987.
- (20) Marquis, S.; Ferrer, B.; Alvalo, M.; Garcia, H.; Roth, H. D. Photoinduced Electron Transfer in Ionic Liquids: Use of 2,4,6-Triphenylpyrilium as a Photosensitizer Probe. *J. Phys. Chem. B* **2006**, *110*, 14956–14960.
- (21) Bräuchle, C.; Lamb, D. C.; Michaelis, J., Eds. *Single Particle Tracking and Single Molecule Energy Transfer*; Wiley-VCH: New York, 2010.
- (22) Fukumura, H.; Irie, M.; Iwasawa, H.; Masuhara, H.; Uosaki, K., Eds. *Molecular Nano Dynamics: Vol. I: Spectroscopic Methods and Nanostructures*; Wiley-VCH: New York, 2009.
- (23) Calzaferri, G. Photonic Antrrnna System for Light Harvesting, Transport and Trapping. *J. Mater. Chem.* **2002**, *12*, 1–13.
- (24) Seebacher, C.; Hellrigel, C.; Bräuchle, C.; Ganschow, M.; Wohrle, D. Orientational Behavior of Single Molecules in Molecular

- Sieves: A Study of Oxazine Dyes in AlPO₄-5 Crystals. *J. Phys. Chem. B* **2003**, *107*, 5445–5452.
- (25) Jung, C.; Hellriegel, C.; Platschek, B.; Wohrle, D.; Bein, T.; Michaelis, J.; Bräuchle, C. Simultaneous Measurement of Orientational and Spectral Dynamics of Single Molecules in Nanostructured Host–Guest Materials. *J. Am. Chem. Soc.* **2007**, *129*, 5570–5579.
- (26) Brühwiler, D.; Calzaferri, G.; Torres, T.; Ramm, J. H.; Gartmann, N.; Dieu, L.-Q.; Lopez-Duarte, I.; Victoria, M.; Martinez-Diaz, M. V. Nanochannels for Supramolecular Organization of Luminescent Guests. *J. Mater. Chem.* **2009**, *19*, 8040–8067.
- (27) Schultz, D. A. Plasmon Resonant Particles for Biological Detection. *Curr. Opin. Biotechnol.* **2003**, *14*, 13–22.
- (28) Hashimoto, S.; Hagiri, M.; Barzykin, A. V. Triplet-Triplet Energy Transfer as a Tool for Probing Molecular Diffusivity within Zeolites. *J. Phys. Chem. B* **2002**, *106*, 844–852.
- (29) Yashonath, S.; Ghorai, P. K. Diffusion in Nanoporous Phases: Size Dependence and Levitation Effect. *J. Phys. Chem. B* **2008**, *112*, 665–686.
- (30) Hashimoto, S.; Miyashita, T.; Hagiri, M. Hypermobility of Aromatic Guest Species in Zeolite as Observed from Anthracene Triplet Self-Quenching within NaY in the Presence of Critical Amounts of Coadsorbed Solvents. *J. Phys. Chem. B* **1999**, *103*, 9149–9155.
- (31) Hashimoto, S.; Ikuta, S.; Asahi, T.; Masuhara, H. Fluorescence Spectroscopic Studies of Anthracene Adsorbed into Zeolites: From the Detection of Cation–π Interaction to the Observation of Dimers and Crystals. *Langmuir* **1998**, *14*, 4284–4291.
- (32) Gartmann, N.; Schutze, C.; Ritter, H.; Brühwiler, D. The Effect of Water on the Functionalization of Mesoporous Silica with 3-Aminopropyltriethoxysilane. *J. Phys. Chem. Lett.* **2010**, *1*, 379–382.
- (33) Hashimoto, S.; Yamashita, S. Visual Observation of Contact-Induced Intercrystalline Migration of Aromatic Species Adsorbed in Zeolites by Fluorescence Microscopy. *ChemPhysChem* **2004**, *5*, 1585–1591.
- (34) Hashimoto, S.; Hagiwara, N.; Asahi, T.; Masuhara, H. Do the Charge-Transfer Complexes of 1,2,4,5-Tetracyanobenzene with Arenes Serve as a Probe for Surveying Chemical Properties Inside the Cavities of Faujasite Zeolites? Time-Resolved and Steady-State Spectroscopic Studies. *Langmuir* **1999**, *15*, 3123–3133.
- (35) Yoon, K. B. Photoinduced Electron Transfer in Zeolites. In *Handbook of Zeolite Science and Technology*; Auerbach, S. M., Carrado, K., Dutta, P. K., Eds.; Marcel Dekker: New York, 2003; pp 591–720.
- (36) Hashimoto, S.; Kiuchi, J. Visual and Spectroscopic Demonstration of Intercrystalline Migration and Resultant Photochemical Reactions of Aromatic Molecules Adsorbed in Zeolites. *J. Phys. Chem. B* **2003**, *107*, 9763–9773.
- (37) Hashimoto, S.; Moon, H. R.; Yoon, K. B. Optical Microscopy Study of Zeolite–Dye Composite Materials. *Microporous Mesoporous Mater.* **2007**, *101*, 10–18.
- (38) Hashimoto, S.; Uwada, T.; Masuhara, H.; Asahi, T. Fabrication of Gold Nanoparticle-Doped Zeolite L Crystals and Characterization by Optical Microscopy: Laser Ablation- and Crystallization Inclusion-Based Approach. *J. Phys. Chem. C* **2008**, *112*, 15089–15093.
- (39) Barzykin, A. V.; Seki, K.; Tachiya, M. Kinetics of Diffusion-Assisted Reactions in Microheterogeneous Systems. *Adv. Colloid Interface Sci.* **2001**, *89–90*, 47–140.
- (40) Ishida, T.; Haruta, M. Gold Catalyst: Towards Sustainable Chemistry. *Angew. Chem., Int. Ed.* **2007**, *46*, 7154–7156.
- (41) Nabika, H.; Takase, M.; Nagasawa, F.; Murakoshi, K. Toward Plasmon-Induced Photoexcitation of Molecules. *J. Phys. Chem. Lett.* **2010**, *1*, 2470–2487.
- (42) Ganschow, M.; Hellriegel, C.; Kneuper, E.; Walk, M.; Thiel, C.; Schultz-Ekloff, G.; Bräuchle, C.; Wöhrle, D. Panchromatic Chromophore Mixtures in an AlPO₄-5 Molecular Sieves: Spatial Separation Effects and Energy Transfer Cascades. *Adv. Funct. Mater.* **2004**, *14*, 269–276.
- (43) Kox, M. H. F.; Stavitski, E.; Weckhuyzen, B. M. Nonuniform Catalytic Behavior of Zeolite Crystals as Revealed by In Situ Optical Microscopy. *Angew. Chem., Int. Ed.* **2007**, *46*, 3652–3655.
- (44) Megelski, S.; Lieb, A.; Pauchard, M.; Drechsler, A.; Glaus, S.; Debus, C.; Meixner, A. J.; Carzaferri, G. Orientation of Fluorescent Dyes in the Nano Channels of Zeolite L. *J. Phys. Chem. B* **2001**, *105*, 25–35.
- (45) Guerrero-Maetinez, A.; Fibikar, S.; Pastoriza-Santos, I.; Liz-Marzan, L. M.; De Cola, L. Microcontainers with Fluorescent Anisotropic Zeolite L Cores and Isotropic Silica Shells. *Angew. Chem., Int. Ed.* **2009**, *48*, 1266–1270.
- (46) Lopez-Duarte, I.; Dieu, L.-Q.; Dolamic, I.; Martinez-Diaz, M. V.; Torres, T.; Carzaferri, G.; Brühwiler, D. On the Significance of the Anchoring Group in the Design of Antenna Materials Based on Phthalocianine Stopcocks and Zeolite L. *Chem.—Eur. J.* **2011**, *17*, 1855–1862.
- (47) De Cremer, G.; Coutino-Gonzalez, E.; Roeffaers, M. B. J.; Moens, B.; Ollevier, J.; Van der Auweraer, M.; Schoonheydt, R.; Jacobs, P. A.; DeSchryver, F. C.; Hofkens, J.; De Vos, D. E.; Vosch, T. Characterization of Fluorescence in Heat-Treated Silver-Exchanged Zeolites. *J. Am. Chem. Soc.* **2009**, *131*, 3049–3056.
- (48) Roeffaers, M. B. J.; Sels, B. F.; Uji-i, H.; Blanpain, B.; L'hoest, P.; Jacobs, P. A.; DeSchryver, F. C.; Hofkens, J.; De Vos, D. E. Space and Time-Resolved Visualization of Acid Catalysis in ZSM-5 Crystals by Fluorescence Microscopy. *Angew. Chem., Int. Ed.* **2007**, *46*, 1706–1709.
- (49) Roeffaers, M. B. J.; Ameloot, R.; Baruah, M.; Uji-i, H.; Bulut, M.; De Cremer, G.; Müller, U.; Jacobs, P. A.; Hofkens, J.; Sels, B. F.; De Vos, D. E. Morphology of Large ZSM-5 Crystals Unraveled by Fluorescence Microscopy. *J. Am. Chem. Soc.* **2008**, *130*, 5763–5772.
- (50) Roeffaers, M. B. J.; Ameloot, R.; Bons, A.-J.; Mortier, W.; De Cremer, G.; de Kloe, R.; Hofkens, J.; De Vos, D. E.; Sels, B. F. Relating Pore Structure to Activity at the Subcrystal Level for ZSM-5: An Electron Backscattering Diffraction and Fluorescence Microscopy Study. *J. Am. Chem. Soc.* **2008**, *130*, 13516–13517.
- (51) Yoon, K. B. Organization of Zeolite Microcrystals for Production of Functional Materials. *Acc. Chem. Res.* **2007**, *40*, 29–40.
- (52) Hashimoto, S.; Hagiri, M.; Matsubara, N.; Tobita, S. Photophysical Studies of Neutral Aromatic Species Confined in Zeolite L: Comparison with Cationic Dyes. *Phys. Chem. Chem. Phys.* **2001**, *3*, 5043–5051.
- (53) Hashimoto, S.; Saitoh, M.; Taira, N.; Schmidt, W.; Hirai, K.; Tomioka, H. Emission Spectroscopic Investigation of Triplet Diarylcarbene Generated in Molecular Sieve VPI-5. *J. Phys. Chem. B* **2005**, *109*, 20407–20414.
- (54) Hashimoto, S.; Yamaji, M. Observation of Intramolecular Singlet and Triplet Excimers of Naphthalene Moieties under the Geometric Constraints Imposed by the Host Framework of Zeolites. *Phys. Chem. Chem. Phys.* **2008**, *10*, 3124–3130.